

Interfacing light and single atoms with a lens

Meng Khoon Tey^a, Syed Abdullah Aljunid^a, Florian Huber^b, Brenda Chng^a, Zilong Chen^c,
Gleb Maslennikov^a and Christian Kurtsiefer^{a,d}

^aCenter for Quantum Technologies, National University of Singapore; Singapore 117543

^bDepartment of Physics, Technical University of Munich; 85748 Munich, Germany

^cInstitute of Materials Research and Engineering; Singapore 117602

^dDepartment of Physics, National University of Singapore; Singapore 117542

ABSTRACT

We investigate the interaction between a single atom and a light field in the strong focusing regime. Such a configuration is subject to recent experimental work not only with atoms but also molecules and other atom-like systems such as quantum dots. We derive the scattering probability for photons by such a microscopic object modeled by a two-level system, starting with a Gaussian beam as the spatial mode of the light field. The focusing by an ideal lens is modeled by adopting a field with spherical wave fronts compatible with Maxwell equations. Using a semi-classical approach for the atom-field interaction, we predict a scattering probability of photons by a single atom of up to 98% for realistic focusing parameters. Experimental results for different focusing strengths are compared with our theoretical model.

Keywords: Atom-light interaction, single atom scattering, strong focusing

1. INTRODUCTION

Atom-light interaction at the single quanta level plays an important role in many quantum communication and computation protocols. While spontaneous emission allows a simple transfer of atomic states into ‘flying’ qubits, strong interaction of light with an atom is needed to transfer a photonic qubit into internal atomic degrees of freedom (stationary qubit). This process is essential to implement quantum light-matter interfaces,¹⁻³ unless post-selection techniques are used.⁴ A measure of interaction strength useful for a variety of physical configurations is the excitation probability of an atom by a single photon, independent of any particular scheme of information transfer from a photon to an atom.

The common approach to achieve this strong interaction pursued for a long time is to use a high finesse cavity around the atom, in which the electrical field strength of a single photon is enhanced by multiple reflections between two highly reflective mirrors, resulting in a high probability of absorption.

Another approach to increase the excitation probability of an atom due to a single photon is simply to focus the light field of a single photon down to a diffraction limited area, motivated by the fact that the absorption cross section of an atom is on the order of the square of the optical wavelength. Recent theoretical research on this matter predicts that the absorption probability may reach the maximal value of 100%⁵ for dedicated focusing geometries. However, the coupling scheme suggested there is challenging to realize experimentally. An alternative scheme would be to use a lens to tightly focus the beam to the position of an atom.

Such a system has been theoretically investigated by van Enk and Kimble⁶ and they concluded that one can expect only low scattering (interaction) probability for lenses with realistic focal lengths. While experiments on single atom absorption have been carried out a long time ago in the weak focusing regime⁷ where this theoretical treatment is applicable, our recent experimental results⁸ showed that the predictions given in their work greatly underestimate the scattering probability of a tightly focused coherent light beam by a single atom. In this paper we extend the model used in⁶ such that it is applicable in the strong focusing regime. We find that, by dropping two of their approximations, the interaction of a coherent light field with a single atom can be very strong even for realistic lenses. Further experimental data is provided for comparison with theoretical predictions.

Corresponding authors: christian.kurtsiefer@gmail.com, mengkhoo.tey@gmail.com

The paper is organized as follows: Section 2 provides the theoretical description of atom-light interaction for a strongly focused light beam. In Section 2.1, we define the scattering probability and express it in terms of the electric field strength at position of the atom. In Section 2.2 we calculate the field strength at the focus of an ideal lens by considering a Gaussian incident beam identical to⁶ but adopting a different description of lens action on the field from the one used in,⁶ using a spherical wave front for the focusing field, and making it compatible with Maxwell equations. From the calculation we obtain a scattering probability for incident photons and compare the results with experimentally measured values in Section 3.

2. THEORY

2.1 Scattering probability of a focused monochromatic beam by a two-level atom

The system that we investigate is a single two-level atom localized in free-space illuminated by a focused monochromatic light field (probe) with an incident power P_{in} . The interaction strength of the probe with the atom is directly related to the amount of incident power that is scattered by the atom. We define the scattering probability of the probe photons by the atom as the ratio of the scattered light power P_{sc} to the total incident power P_{in} , i.e.

$$p_{\text{sc}} \equiv \frac{P_{\text{sc}}}{P_{\text{in}}}, \quad (1)$$

where P_{sc} is defined by (34) which represents the average optical power spontaneously emitted by a two-level system exposed to a monochromatic light field. The expression for the scattered power is commonly obtained using the steady state solutions of the optical Bloch equations.¹³

We now derive an expression for the scattering probability of a focused Gaussian beam by a two-level atom assuming weak on-resonant excitation, making use of the fact that the atom only interacts with the field at the location of the atom in the long wavelength limit. We consider a circularly polarized Gaussian beam since it was adopted in the experiment.⁸ Assuming that the waist of the beam coincides with the lens and the beam propagates along the +Z axis, the electric field strength before the focusing lens is given by

$$\vec{E}(\rho, t) = \frac{E_L}{\sqrt{2}} [\cos(\omega t)\hat{x} + \sin(\omega t)\hat{y}] e^{-\rho^2/w_L^2}, \quad (2)$$

where ρ is the radial distance from the lens axis, w_L the waist of the beam, \hat{x}, \hat{y} are the unit vectors in X and Y directions respectively, and E_L is the field amplitude. The total power carried by the incident beam is given by

$$P_{\text{in}} = \frac{1}{4}\epsilon_0\pi c E_L^2 w_L^2, \quad (3)$$

where ϵ_0 is the electric permittivity of vacuum, and c the speed of light in vacuum. Due to the symmetry of the system, the field on the lens axis is always circularly polarized. So for an atom that is stationary on the z-axis at the focus of the lens, the electric field can be written as

$$\vec{E}(t) = \frac{E_A}{\sqrt{2}} [\cos(\omega t)\hat{x} + \sin(\omega t)\hat{y}], \quad (4)$$

where E_A denotes the amplitude of the field at the focus. For a field that is resonant with the atomic transition and with an intensity much below saturation, the power scattered by a two-level atom is¹³ (see A for more details)

$$P_{\text{sc}} = \frac{3\epsilon_0 c \lambda^2 E_A^2}{4\pi}, \quad (5)$$

leading to a scattering probability for photons of

$$p_{\text{sc}} = \frac{P_{\text{sc}}}{P_{\text{in}}} = \frac{3\lambda^2}{\pi^2 w_L^2} \left(\frac{E_A}{E_L} \right)^2. \quad (6)$$

(6) is exact under weak and on-resonant excitation. For a weakly focused field where the paraxial approximation holds one finds that

$$\left(\frac{E_A}{E_L}\right)^2 = \left(\frac{w_L}{w_f}\right)^2, \quad (7)$$

where w_f is the Gaussian beam waist at the focus. This leads to the following expression for the scattering probability:

$$p_{sc} = \frac{3\lambda^2}{\pi^2 w_f^2}. \quad (8)$$

One can see that by defining a Gaussian focal spot area $A = \pi w_f^2/2$, (8) leads to $p_{sc} = \sigma_{\max}/A$, where $\sigma_{\max} = 3\lambda^2/2\pi$ is the absorption cross section of a two-level system exposed to a resonant plane wave. However, for strongly focused light, the paraxial approximation breaks down, and we need other methods to find $(E_A/E_L)^2$.

2.2 Calculation of electric field strength after the lens

A useful method to calculate the field strength after an ideal lens was presented by van Enk and Kimble in.⁶ The main idea of their method is to first assume a focusing field near the exit of the lens, taking into account the focusing effects of an ideal lens. They then decomposed the focusing field into a set of modes that takes a simple form in the cylindrical coordinates, thus making use of the symmetry of the system. Once the contribution of each mode is known, the full properties of the field after the lens can be determined with certainty. Unfortunately, their description for the focusing field near the lens is only suitable for weak focusing. In this section we extend their model such that it becomes applicable to the strong focusing regime. The extension is done by modeling the lens action such that the focusing field has a spherical wave front after the lens and is compatible with Maxwell equations. Thus the model is now applicable for description of lenses with high numerical aperture (NA).

2.2.1 Decomposition of the field into modes with cylindrical symmetry

We briefly outline the main properties of the cylindrical modes, directly following.⁶ The complete orthogonal set of modes \vec{F}_ν is defined such that an electric field that satisfies the source-free Maxwell equations can be expanded in these modes as

$$\vec{E}(t) = 2\Re \left[\sum_\nu a_\nu \vec{F}_\nu e^{i\omega t} \right], \quad (9)$$

where the summation over ν is a short-hand notation for

$$\sum_\nu \equiv \int dk \int dk_z \sum_s \sum_m, \quad (10)$$

and a_ν are arbitrary complex amplitudes. The modes are characterized by four indices $\nu \equiv (k, k_z, m, s)$, where $k = \frac{2\pi}{\lambda}$ is the wave vector modulus, $k_z = \vec{k} \cdot \hat{z}$ the wave vector component in z -direction, m an integer-valued angular momentum index, and $s = \pm 1$ the helicity.

Since the electrical field has to satisfy Maxwell equations, the mode function should be transverse, i.e., $\nabla \cdot \vec{F}_\nu = 0$. The dimensionless mode functions \vec{F}_ν in cylindrical coordinates (ρ, z, ϕ) are defined in⁹ as

$$\begin{aligned} \vec{F}_\nu(\rho, z, \phi) = & \frac{1}{4\pi} \frac{sk-k_z}{k} G(k, k_z, m+1) \hat{e}_- + \frac{1}{4\pi} \frac{sk+k_z}{k} G(k, k_z, m-1) \hat{e}_+ \\ & - i \frac{\sqrt{2}}{4\pi} \frac{k_t}{k} G(k, k_z, m) \hat{z}, \end{aligned} \quad (11)$$

where $k_t = \sqrt{k^2 - k_z^2}$ is the transverse part of the wave vector, $\hat{e}_\pm = (\hat{x} \pm i\hat{y})/\sqrt{2}$ are the two circular polarization vectors, and

$$G(k, k_z, m) = J_m(k_t \rho) e^{ik_z z} e^{im\phi}, \quad (12)$$

with J_m the m -th order Bessel function. As we are interested in a monochromatic beam with a fixed value of $k = 2\pi/\lambda$ propagating in the positive z direction ($k_z > 0$), the set of mode indices is reduced to $\mu \equiv (k_t, m, s)$ where, for convenience, k_t is taken as a mode index instead of k_z . Now, we introduce the notation

$$\sum_\mu \equiv \int dk_t \sum_s \sum_m \quad (13)$$

for a complete summation over all possible modes. For a fixed k the modes \vec{F}_μ are orthogonal in planes perpendicular to the z axis:

$$\int dS \vec{F}_\mu^*(\vec{r}) \cdot \vec{F}_{\mu'}(\vec{r}) = \delta(k_t - k'_t) \delta_{mm'} \delta_{ss'} / (2\pi k_t), \quad (14)$$

where dS is a surface element on such a plane.

2.2.2 Focusing with an ideal lens

Similar to⁶ we start modeling an ideal lens by multiplying a local phase factor $\varphi(\rho)$ to the incoming field \vec{F}_{in} . As in Section 2.1, we consider a collimated circularly polarized Gaussian beam which is focused by an ideal lens in the plane $z = 0$. In the new notations, the dimensionless incoming field is given by

$$\vec{F}_{\text{in}} = \exp\left(-\frac{\rho^2}{w_L^2}\right) \hat{e}_+, \quad (15)$$

and the output field right after the lens is modeled by

$$\vec{F}_{\text{out}}(\rho, \phi, z = 0) = \varphi(\rho) \exp\left(-\frac{\rho^2}{w_L^2}\right) \hat{e}_+. \quad (16)$$

The complete output field is then obtained by

$$\vec{F}_{\text{out}}(\vec{r}) = \sum_{\mu} \kappa_{\mu} \vec{F}_{\mu}(\vec{r}), \quad (17)$$

with

$$\kappa_{\mu} = 2\pi k_t \int_{z=0} dS \vec{F}_{\text{out}}(\vec{r}) \cdot \vec{F}_{\mu}^*(\vec{r}). \quad (18)$$

Now one has to choose an appropriate phase factor $\varphi(\rho)$ to describe the action of the lens on the incoming field. In the original paper⁶ the local phase factor was chosen to be

$$\varphi_{\text{pb}}(\rho) = e^{-ik\rho^2/2f}, \quad (19)$$

where f is the focal length of the lens. This phase factor gives rise to a parabolic wave front after the lens for small ρ . The choice of this phase factor allows an analytical integration for obtaining the coefficients κ_{μ} but does not apply for description of lenses with high numerical aperture. Moreover, in our recent experiment much higher values of extinction than that predicted with the help of (19) were directly measured.⁸ This motivates us to adopt a different description for the focusing field.

Light emitted by a small object like an atom has a spherical wave front in the far field. One can thus expect that the lens has to reverse the spherical emission in order to direct most of the incoming energy into the focal region around the atom. Therefore, we describe action of the lens with a phase factor

$$\varphi_{\text{sp}}(\rho) = e^{-ik(\sqrt{\rho^2+f^2}-f)}, \quad (20)$$

which is expected to create a focusing field with a spherical wave front after the lens. Note that φ_{sp} approaches φ_{pb} for small ρ . With phase factor φ_{sp} the expansion coefficient κ_{μ} becomes

$$\kappa_{\mu} = \delta_{m1} \pi k_t \frac{sk + k_z}{k} \int_0^{\infty} d\rho \left[\rho J_0(k_t \rho) \times e^{-ik(\sqrt{\rho^2+f^2}-f)-\rho^2/w_L^2} \right]. \quad (21)$$

This integration has no analytical solution and thus is computed numerically. As one of the mode indices k_t is a continuous variable, a sufficiently large number of κ_{μ} must be first computed and then interpolated in order to construct the output field correctly. The largest component of the output field (17) is the \hat{e}_+ component, which is given by

$$F_+(\rho, \phi, z) = \frac{1}{4\pi k} \sum_{s=\pm 1} \int_0^k dk_t \left[(sk + k_z) J_0(k_t \rho) \times e^{ik_z z} \kappa_{\mu=(k_t, 1, s)} \right], \quad (22)$$

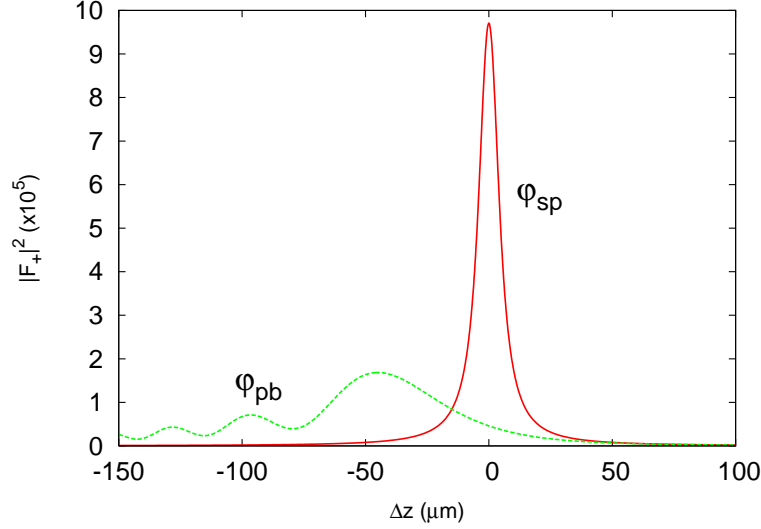


Figure 1. $|F_+|^2$ along the lens axis obtained with a spherical phase factor φ_{sp} and a parabolic phase factor φ_{pb} for the parameters mentioned in the text.

where $F_+ \equiv \vec{F}_{out} \cdot \hat{e}_+^*$, and \hat{e}_+^* is the complex conjugate of \hat{e}_+ .

Figure 1 shows the near-focus dimensionless intensity $|F_+|^2$ obtained for the parameters: $f = 4.5$ mm, $\lambda = 780$ nm and $w_L = 1.1$ mm, using the phase factors φ_{sp} (solid line) and φ_{pb} (dashed line) respectively. The horizontal axis shows the displacement from the ideal focal position along the lens axis $\Delta z = z - f$. It is clear from the figure that adopting a parabolic wave front significantly reduces the maximal intensity behind the lens. Unlike φ_{sp} which concentrates the energy of the field in a small region, φ_{pb} spreads the energy of the focused field over a region closer to the lens, and thus results in a reduced intensity in the focus similar to spherical aberration in classical optics. This problem becomes more serious for a larger input waist w_L (or stronger focusing) because a parabolic wave front deviates more from a spherical wave front for larger ρ . The numerical result for $|F_+|^2$ allows calculation of the scattering probability using (6). With

$$\left(\frac{E_A}{E_L}\right)^2 = |F_+|^2 \quad (23)$$

we obtain a value for p_{sc} of 14.8% for a spherical phase factor φ_{sp} , whereas the parabolic phase factor adopted in⁶ only leads to a scattering probability of 2.6%.

2.2.3 Focusing field compatible with Maxwell equations

As one can see from Figure 1, adoption of the spherical phase factor $\varphi_{sp}(\rho)$ predicts a higher intensity at the focus. However, an initial outgoing field near the lens modeled with the help of (16) is not compatible with Maxwell equations for two reasons: (i) the power carried by this field directly behind the lens was found to be different from the total power flowing through the focus; (ii) the complete outgoing field $\vec{F}_{out}(\vec{r})$ obtained through Equations (17) and (18) has non-vanishing \hat{z} and \hat{e}_- components at $z = 0$ even though the initial outgoing field we start with only has the \hat{e}_+ component. Such discrepancies are negligible for small w_L , but become very large for large w_L .

To be more precise, the reconstructed field (17) must satisfy Maxwell equations since it is a linear combination of \vec{F}_ν which themselves are the solutions of source-free Maxwell equations. If the reconstructed field is not identical to the initial field, then the initial field cannot satisfy Maxwell equation, and vice versa. Therefore, (16) cannot represent a physical field.

In view of this, we model the field right after the lens by considering changes in local polarization on top of using the spherical phase factor with three requirements in mind. The requirements are: (i) A rotationally

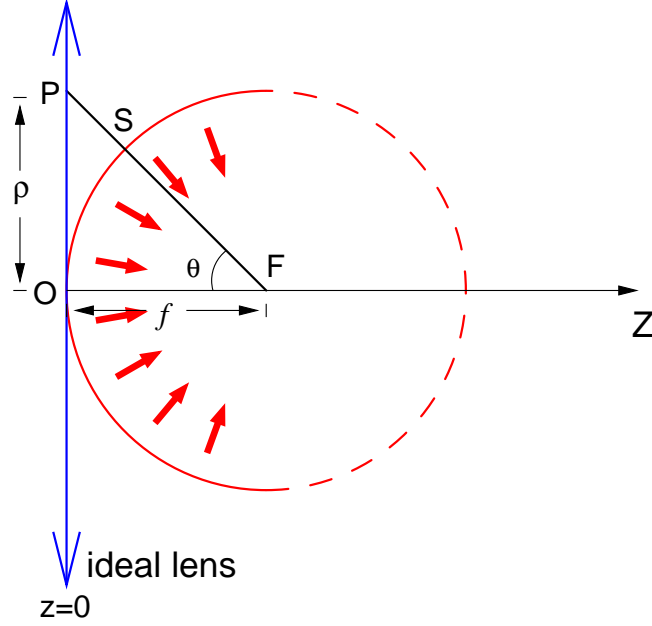


Figure 2. A spherical wave front (half of the sphere) formed after passing an ideal thin lens. Here F is the focal point of the lens, f is the focal length, S is the intercept point of line PF and the wave front.

symmetric lens does not alter the local azimuthal field component, and only tilts the local radial polarization component of the incoming field towards the axis; (ii) The polarization at point P (see Figure 2) after transformation by the lens should be orthogonal to the line FP to form a spherical wave front; (iii) The modulus of the local field strength before and after the lens should be the same, so that the local intensity of the outgoing field is the same as that of the incoming Gaussian beam. These requirements are identical to the assumptions made by Richards and Wolf on the transformation of polarization of optical rays by optical elements.¹⁰ With these requirements, we model the field right after the lens as (see B for details)

$$\vec{F}_{\text{out}}(\rho, \phi, 0) = \left(\frac{1+\cos\theta}{2} \hat{e}_+ + \frac{\sin\theta e^{i\phi}}{\sqrt{2}} \hat{z} + \frac{\cos\theta-1}{2} e^{2i\phi} \hat{e}_- \right) \exp(-\rho^2/w_L^2) \times \exp\left[-ik(\sqrt{\rho^2+f^2}-f)\right]. \quad (24)$$

The expansion coefficient κ_μ (18) becomes

$$\kappa_\mu = \delta_{m1} \pi k_t \int_0^\infty d\rho \rho \left\{ \frac{sk+k_z}{k} \left(\frac{1+\cos\theta}{2} \right) J_0(k_t \rho) + i \frac{\sqrt{2} k_t}{k} \left(\frac{\sin\theta}{\sqrt{2}} \right) J_1(k_t \rho) + \frac{sk-k_z}{k} \left(\frac{\cos\theta-1}{2} \right) J_2(k_t \rho) \right\} \exp\left[-ik(\sqrt{\rho^2+f^2}-f) - \frac{\rho^2}{w_L^2}\right], \quad (25)$$

where $\theta = \tan^{-1}(\rho/f)$. The Kronecker symbol δ_{m1} expresses the fact that the angular momentum of the incident light beam is still conserved under the new transformation we use.^{11,12} Finally, we determine the complete outgoing field with three polarization components defined by $F_+ \equiv \vec{F}_{\text{out}} \cdot \hat{e}_+$, $F_z \equiv \vec{F}_{\text{out}} \cdot \hat{z}$, and $F_- \equiv \vec{F}_{\text{out}} \cdot \hat{e}_-$, with

$$F_+(\rho, \phi, z) = \sum_{s=\pm 1} \int_0^k dk_t \frac{1}{4\pi} \frac{sk+k_z}{k} J_0(k_t \rho) e^{ik_z z} \kappa_\mu, \quad (26)$$

$$F_z(\rho, \phi, z) = \sum_{s=\pm 1} \int_0^k dk_t (-i) \frac{\sqrt{2} k_t}{4\pi k} J_1(k_t \rho) e^{ik_z z} e^{i\phi} \kappa_\mu, \quad (27)$$

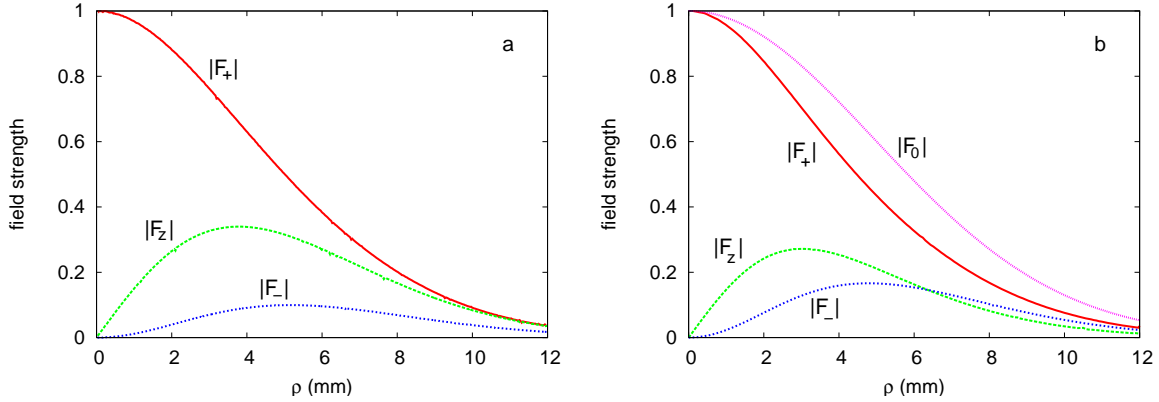


Figure 3. Absolute field strengths after the ideal lens reconstructed from the expansion into cylindrical components at $z = 0$ obtained with parameters: $f = 4.5$ mm, $\lambda = 780$ nm, and $w_L = 7$ mm. (a) Polarization-corrected outgoing field given by (24). (b) Only with spherical wave front phase factor φ_{sp} , no polarization correction. The traces are: the amplitude of the original \hat{e}_+ -polarized field $|F_0|$, and the reconstructed field strengths $|F_+|$, $|F_z|$ and $|F_-|$.

$$F_-(\rho, \phi, z) = \sum_{s=\pm 1} \int_0^k dk_t \frac{1}{4\pi} \frac{sk - k_z}{k} J_2(k_t \rho) e^{ik_z z} e^{2i\phi} \kappa_\mu. \quad (28)$$

We now consider a set of focusing parameters, say $f = 4.5$ mm, $\lambda = 780$ nm, and $w_L = 7$ mm, for which the incident beam is strongly focused by the lens. We reconstruct the field after passage through the lens at $z = 0$ using Equations (26), (27), and (28) and compare it to the starting output field given by Equation (24) that is corrected for polarization. Figure 3a shows (from top to bottom) the reconstructed $|F_+|$, $|F_z|$ and $|F_-|$ at $z = 0$. As the reconstructed fields overlap visually with the polarization-corrected field behind the lens, the original field distributions are not shown. Quantitatively, the relative difference between the original and reconstructed field is less than 10^{-3} , a bound limited by our numerical accuracy. For comparison, the reconstructed fields obtained using φ_{sp} without polarization correction are shown in Figure 3b. The reconstructed fields at $z = 0$ are not the same as the original field $|F_0|$ we start with. A successful reconstruction, therefore, shows that our extended model (24) is physical (compatible with Maxwell equations) even for very strong focusing**.

Another check that further confirms this is that the total energy carried by the field is conserved after the lens. To verify this we compare the power flowing through the focus to the incoming power at the lens. The power flowing through the focus is obtained from

$$P(z) = 2\pi \int_0^{\rho_0} d\rho \rho (|F_+(z)|^2 + |F_z(z)|^2 + |F_-(z)|^2) \quad (29)$$

by setting $z = f$. We find that a power flowing through the focus is only 0.02% less than the incoming power for this set of parameters that provide the strongest focusing for the polarization-corrected field (Figure 3a). If we only adopt the spherical phase factor without polarization correction, the power at the focus is only $\simeq 78\%$ of the incident power for the same set of focusing parameters. This check provides further evidence that (24) gives a physical focusing field after the lens.

2.2.4 Field at the focus

Having found a field with a spherical wave front that is compatible with Maxwell equations, we can now examine the field at the focus in more details. Figure 4 shows the field on the focal plane for different focusing strengths

**In principle, since we can only tell that the reconstructed fields coincides with the initial fields within our numerical accuracy, we cannot prove that (24) satisfies Maxwell equations. In any case, we confirm that (24) is at least a very good approximation to a physical field for all parameters we have used in this report, namely, $f = 4.5$ mm and w_L from 0.1 mm to 10 mm.

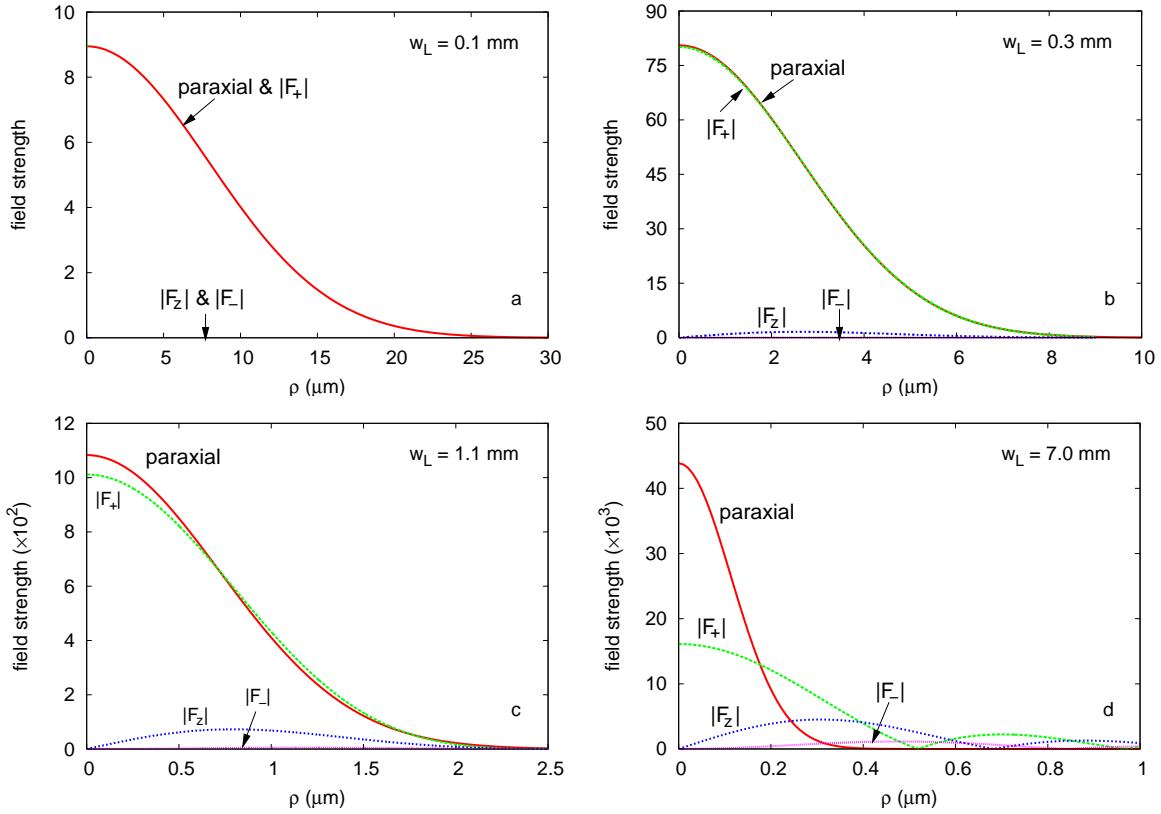


Figure 4. Absolute field strengths at the focus for different focusing strengths. Different plots are obtained with the same focal length of 4.5 mm and wavelength of 780 nm, but with different input waist w_L .

obtained with this model. Every individual plot in the figure assumes the same focal length ($f=4.5$ mm) and wavelength ($\lambda=780$ nm), but with different input waists w_L . In each plot, we show the absolute field strengths $|F_+|$, $|F_z|$, and $|F_-|$, together with the field predicted using paraxial approximation given by

$$\vec{F}_{\text{focus}}^{\text{parax}} = \frac{w_L}{w_f} \exp\left(-\frac{\rho^2}{w_f^2}\right) \hat{e}_+, \quad (30)$$

with a paraxial focal waist $w_f = f\lambda/\pi w_L$. For weak focusing, $|F_+|$ overlaps completely with the paraxial prediction with negligible $|F_z|$ and $|F_-|$ (Figure (4a)). For $w_f \simeq 3.7\mu\text{m}$ (about 5λ), discrepancies between paraxial approximation and the extended model start to appear (Figure (4b)). The \hat{z} - and \hat{e}_- -polarized fields become stronger when w_L gets larger. However, they never appear on the lens axis. Therefore, an atom localized on the lens axis would only experience the \hat{e}_+ -polarized field. Figure 4d shows the focused field that maximizes $|F_+|$ for the parameters in our model. It is obtained with a incident waist $w_L = 7$ mm. Increasing the incident waist further can no longer make the focal spot tighter due to the diffraction limit. Instead, more energy is transferred to the $|F_z|$ and $|F_-|$ side lobes, thus decreasing the magnitude of the $|F_+|$ component again.

It should also be noted that a strongly focused field does not have a planar wave front at the focus. This can be understood from the fact that

$$F_z(\rho, \phi, z) = F_z(\rho, z)e^{i\phi}, \text{ and } F_-(\rho, \phi, z) = F_-(\rho, z)e^{2i\phi}, \quad (31)$$

which means the phase of the field on the focal plane $z = f$ is not uniform (Equations (27) and (28)).

2.2.5 Scattering probability

Once we know the field at the focus, we can obtain the scattering probability of a light beam by a two-level atom. Figure 5 displays the scattering probability as a function of incident waist w_L , obtained for focusing

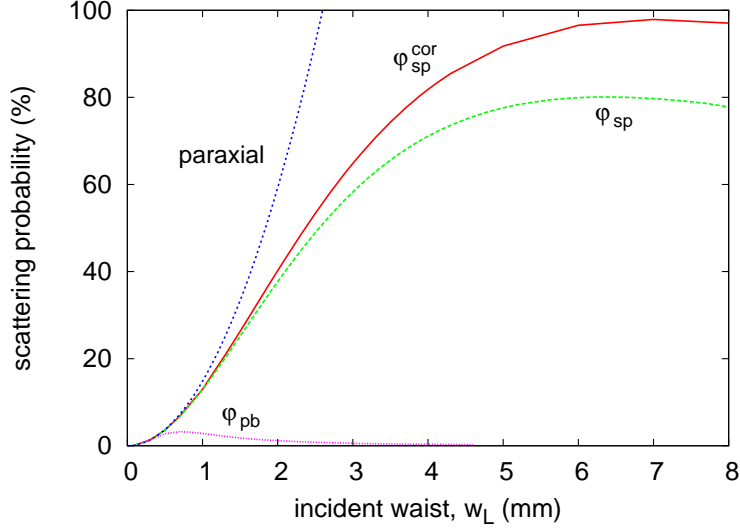


Figure 5. Scattering probability as a function of w_L obtained (from top to bottom) by assuming paraxial approximation, spherical wave front with polarization correction, spherical wave front without polarization correction, and parabolic wave front without polarization correction.

parameters $f = 4.5$ mm, $\lambda = 780$ nm. The curves in the figure are obtained using (from top to bottom) paraxial approximation (Equation (30)), spherical wave front with polarization correction (Equation (24)), spherical wave front without polarization correction (Equations (16) and (20)), and parabolic wave front without polarization correction (Equations (16) and (19)). It is clear that adopting a parabolic wave front after the lens only leads to a small scattering probability (φ_{pb} curve). With a spherical wave front, the scattering probability increases significantly especially for stronger focusing (φ_{sp} curve). However, as was pointed out in the previous sections, modeling the output field without considering the action of the lens on the polarization of the field gives rise to an unphysical focusing field. Our attempt to construct a physical focusing field predicts even larger scattering probability with a maximal value of $\simeq 98\%$ (φ_{sp}^{cor} curve). It should be noted that all three models agree with the paraxial model for small w_L . For large w_L , the parabolic model shows the largest discrepancy with respect to the physical field model. The result obtained shows that a scattering probability should be high enough to be directly measured in a simple transmission experiment with realistic, readily available lenses.

3. EXPERIMENT

In this section, we report the results of our experiment which tries to quantify the scattering probabilities of light fields with different focusing strengths by a single ^{87}Rb atom. Obtaining the scattering probability defined by (1) is not straightforward in an experiment. Normally, the total incident power of the probe P_{in} can be measured directly. However, measuring the total scattered power P_{sc} is challenging since the detection area must cover the whole solid angle, including that subtended by the probe beam. A simpler method for quantifying the scattered power is to infer it from a transmission measurement. Figure 6 illustrates a simple transmission setup with an atom located at the focus of two confocal lenses. There, a second lens collects all the excitation power if no atom is present at the focus. For an optical power measuring device, the measured transmission is defined as the ratio of the outgoing power P_{out} to the incident power P_{in} . Considering from the perspective of balancing the optical powers, one can relate the measured transmission T to the scattered power P_{sc} by

$$T \equiv \frac{P_{out}}{P_{in}} = \frac{P_{in} - P_{sc} + \alpha P_{sc}}{P_{in}}, \quad (32)$$

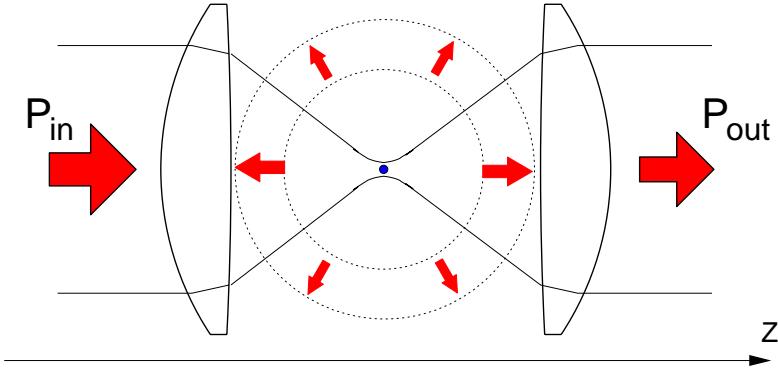


Figure 6. A transmission measurement setup with an atom at the focus of a lens. The transmitted power is a result of interference between the scattered light and the probe for coherent scattering.

where α is a factor related to the solid angle subtended by the power detector area. The scattering probability is then related to the measured transmission by

$$p_{sc} = \frac{\epsilon}{1 - \alpha}, \quad (33)$$

where $\epsilon = 1 - T$ is the extinction of the probe beam.

A more accurate description of this transmission measuring system requires consideration of the interference between the attenuated probe and the coherently scattered field in order to obtain the value of α . Finding α or the exact relation between the scattering probability and the measured extinction is complicated and not the focus of our current discussion. We note in passing that if the solid angle subtended by the probe beam is small, most of the scattered field is directed out of the probe mode. In this case, $|\alpha|$ is expected to be much smaller than one, and thus $p_{sc} \approx \epsilon$. Since the solid angle subtended by the transmission collecting lens used in our experiment is less than $0.06 \times 4\pi$, we expect that our measured extinction to be comparable with the actual scattering probability of the light beam by the atom.

A detailed description of our single atom transmission experiment is reported in.⁸ Here, we give a brief outline of the setup and report the measured extinction values for different focusing strengths by changing the input waist of the probe beam. Figure 7 shows the experimental setup. The heart of the setup consists of two aspheric lenses that are mounted in a UHV chamber in a confocal arrangement. A single ^{87}Rb atom is localized in a far-off resonant dipole trap (FORT) that is formed by 980 nm light at the focus of the lens system. A probe beam is delivered from a single-mode fiber and focused onto the atom by one of the aspheric lenses. The confocal arrangement of lenses ensures that the second lens picks up all the incident probe power, thus implementing the scheme discussed in Section 2.1. We use a circularly polarized probe to optically pump the atom into a closed cycling transition. This procedure effectively ensures that the atom can be viewed as a two-level system during interaction with the probe, so that a maximal scattering probability can be expected. After allowing some time for optical pumping, we measure the transmission of the probe beam that is defined as the ratio of count rates at detector D1 when the atom is present in the trap, to the count rate when the atom is absent. Such a measurement is carried out for different probe frequencies and the transmission spectrum of a single Rb atom is obtained. The spectrum is fitted to a Lorentzian from which we obtain three parameters: the resonant frequency, full width at half maximum (FWHM) of the transmission spectrum and the minimum value for the transmission T_{\min} at resonance frequency. We obtained transmission spectra for four different input waists of the probe, thus measuring extinction for different focusing strengths. For all measured spectra the observed FWHM did not exceed 7.7 MHz, which is close to the natural linewidth of the transition that we addressed (6 MHz). From that we conclude that during the measurement, the atom was successfully kept in the cycling two-level system. During each transmission measurement at all frequencies of the probe, the probe power was maintained at a level much below saturation, such that the atom scatters ≈ 2500 photons per second. The properties of various transmission spectra obtained with different probe incident waists are summarized in Table 1.

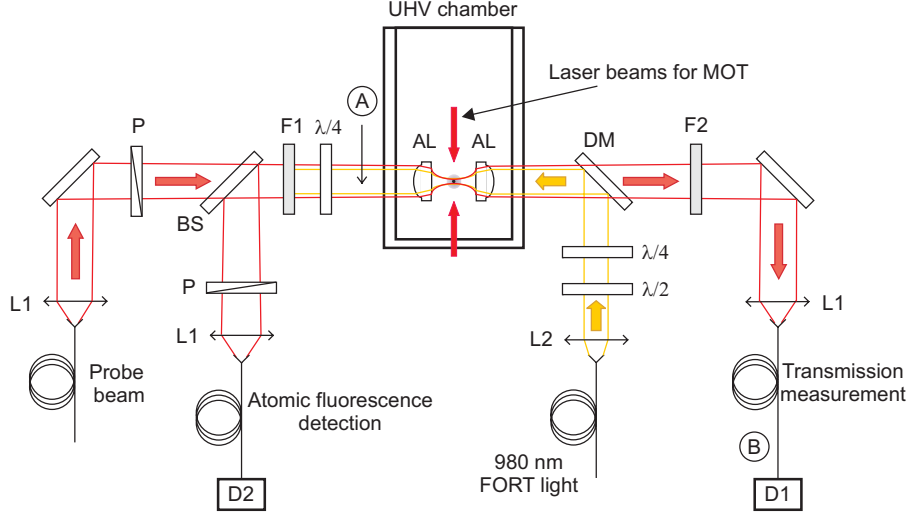


Figure 7. Experimental setup for measuring the extinction of a light beam by a single atom. AL: aspheric lens ($f = 4.5$ mm, full NA = 0.55), P: polarizer, DM: dichroic mirror, BS: beam splitter with 99% reflectivity, $\lambda/4$, $\lambda/2$: quarter and half wave plates, F1: filters for blocking the 980 nm FORT light, F2: interference filter centered at 780 nm, D1 and D2: Si-avalanche photodiodes. Four more laser beams forming the MOT lie in an orthogonal plane and are not shown.

We also carefully characterized the losses of the probe beam in its optical path to ensure that our measured extinctions are not exaggerated by interference artefacts that can happen when certain elements in the transmission path preferentially filter more probe than the scattered light.⁸ From point A to point B in Figure 7 we measured 53–60% transmission without the atom in the trap. The losses are mostly determined by 21% loss through the uncoated UHV chamber walls and 17–24% loss due to the coupling into the single-mode fiber at the transmission measurement channel. The loss at the coupling into the fiber increases as the input waist of the probe beam w_L increases. Almost all losses can be ascribed to reflections at optical surfaces, except for a 9–16% re-coupling loss into a single mode fiber that is due to mode mismatch. We are thus reasonably confident that our measurement is free from artefacts that may arise due to improper collection of the probe.

4. DISCUSSION

In Figure 8 we compare the extinctions obtained from the experiment with scattering probability predicted using the models presented in Section 2. However, we do not have yet a clear model that relates the measured extinction to the scattering probability. We suspect that the measured extinction is comparable to the actual scattering probability in our experiment according to the previous discussion. Following this assumption, we see that adoption of the spherical phase factor with polarization correction predicts larger values of the scattering probability than that observed in the experiment. We see a few possible reasons for this discrepancy. First of all, the lens used in the experiment can show some aberrations, and the intensity distribution of the focusing field after the lens might also be different from (24) due to the finite thickness of a real lens. Besides, the motion of the

w_L (mm)	w_f (μm)	w_D (μm)	ϵ_{max} (%)	W (MHz)	$p_{\text{sc}}^{\text{calc}}$ (%)
0.5	2.23	2.0	2.38 ± 0.03	7.1 ± 0.2	3.59
1.1	1.01	2.0	7.2 ± 0.1	7.4 ± 0.2	15.6
1.3	0.86	1.4	9.8 ± 0.2	7.5 ± 0.2	20.8
1.4	0.80	1.4	10.4 ± 0.1	7.7 ± 0.2	23.5

Table 1. Summary of transmission spectra of the probe for different focusing strengths. w_L : incident waist of the probe; w_f and w_D : estimated focal waists of the probe and of the FORT respectively using paraxial approximation; ϵ and W: maximum observed extinction value and FWHM of the transmission spectrum respectively. The scattering probability $p_{\text{sc}}^{\text{calc}}$ is calculated using the physical focusing field with a spherical wave front (24) for the corresponding waist.

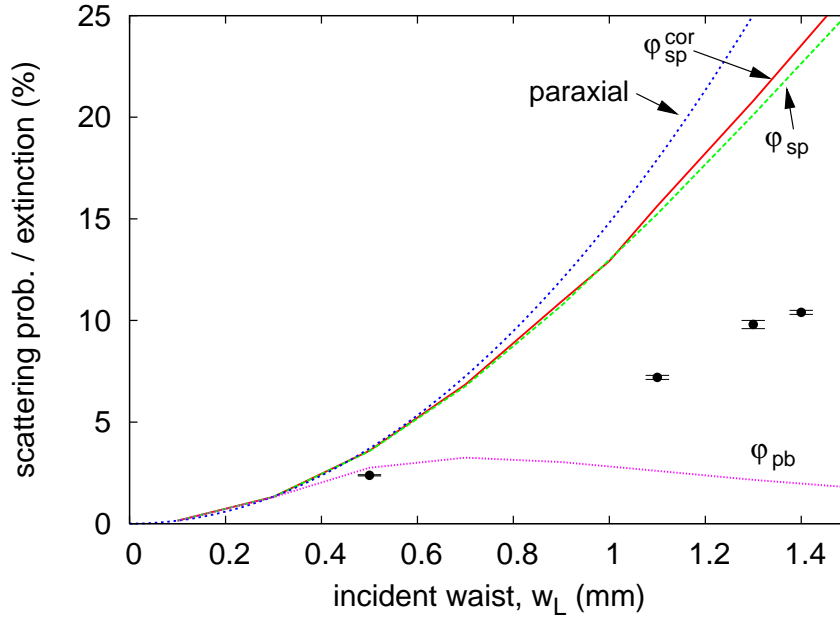


Figure 8. Comparison of experimentally obtained extinction values to scattering probabilities predicted by various models mentioned in the text.

atom in the dipole trap also results in reduced scattering probability. Finally, to obtain the field at the location of the atom, we expanded the incident field into modes that satisfy source-free Maxwell equations. However, the single atom itself acts as a microscopic current source that can influence the field. For strong focusing where a large scattering probability is achieved, obtaining the field using source-free Maxwell equations may not be justified.

Another approach to describe the system we are investigating is to use the ‘overlap’ argument for the calculation of the scattering probability.^{5,14} The approach is based on the time reversibility of the Schrödinger equation under the assumption of a closed ‘atom+field’ system. A scattering probability of 100% is predicted for an incoming photon that is prepared as a time-reversed replica of the spontaneously emitted photon. In order to match the spatial overlap with the spontaneously emitted photon, a probing photon must occupy the full solid angle of 4π . This suggests, that by using an infinitely large lens, a scattering probability of only 50% may be expected since the collection solid angle of the lens is equal to 2π . This contradicts the result of our calculation, which suggests that a scattering probability of more than 50% can be achieved even if the atom is excited by a field that is focused from solid angle less than 2π . An experiment with a lens of higher NA can test the applicability of both models.

5. CONCLUSION

We have demonstrated both theoretically and experimentally that a substantial coupling efficiency of a light beam to a single atom can be achieved by focusing a light beam with a lens. By modifying the model given in,⁶ we have constructed a field compatible with Maxwell equations after the lens that is suitable for the strong focusing regime. High values for the scattering probability of light (up to 98%) by a two-level atom stationary at the focus under the assumption of weak on-resonant coherent probe are predicted. Experimental results confirm the possibility of observing a substantial coupling efficiency. These results may also be of interest for experiments with single molecules^{15,16} and quantum dots.¹⁷

ACKNOWLEDGMENTS

This work was partly supported by the National Research Foundation, the Ministry of Education, Singapore, and by FRC grant R-144-000-174-112. During the preparation of this manuscript, related work by Zumofen et al.¹⁸ appeared which investigates the interaction of a two-level system with various other focusing field configurations, and where interference between excitation and scattered light is considered.

APPENDIX A. POWER SCATTERED BY THE ATOM IN COHERENT LIGHT FIELD

Using optical Bloch theorem, it can be shown that the average power scattered by a two-level atom exposed to a monochromatic light beam is given by¹³

$$P_{sc} = \rho_{22}\Gamma\hbar\omega, \quad (34)$$

where ρ_{22} is the excited state population and Γ is the spontaneous decay rate, such that $\dot{\rho}_{22} = -\Gamma\rho_{22}$ in the absence of an external light field. The excited state population and its spontaneous decay rate are related to the atomic dipole moment $|d_{12}|$ and the amplitude of the field at the location of the atom E_A (Equation (4)) by

$$\rho_{22} = \frac{|\Omega|^2/4}{\delta^2 + |\Omega|^2/2 + \Gamma^2/4}, \quad (35)$$

$$\Gamma = \frac{\omega_{12}^3|d_{12}|^2}{3\pi\epsilon_0\hbar c^3}, \quad (36)$$

where $\Omega = E_A|d_{12}|/\hbar$ is the resonant Rabi frequency and $\delta = \omega - \omega_{12}$ is the detuning of the driving field frequency ω from the atomic two-level resonance frequency ω_{12} . These formulas are obtained using the dipole approximation of the interaction Hamiltonian and the rotating wave approximation. For a weak ($\Omega \ll \Gamma$) on resonant ($\delta = 0$) excitation, the scattered power (Equation (34)) becomes

$$P_{sc} = \frac{3\epsilon_0 c \lambda^2 E_A^2}{4\pi}. \quad (37)$$

APPENDIX B. TRANSFORMATION OF LOCAL POLARIZATION BY THE LENS

To obtain the local polarization of the focusing field in (24), we consider an arbitrary point P($\rho, \phi, 0$) before the lens and an incident light field with polarization

$$\hat{\epsilon}_{in} = \hat{\epsilon}_+ = \frac{\hat{x} + i\hat{y}}{\sqrt{2}}, \quad (38)$$

or in the cylindrical basis,

$$\hat{\epsilon}_{in} = \frac{e^{i\phi}}{\sqrt{2}} \hat{\rho} + \frac{ie^{i\phi}}{\sqrt{2}} \hat{\phi}, \quad (39)$$

where $\hat{\rho} = \cos\phi \hat{x} + \sin\phi \hat{y}$ and $\hat{\phi} = -\sin\phi \hat{x} + \cos\phi \hat{y}$ are two unit vectors along the radial and azimuthal directions respectively. The ideal lens leaves the azimuthal component unchanged but tilts the radial component such that the local polarization of the field right after the lens is perpendicular to the line FP in Figure 2 (F is the focus point), that is:

$$\begin{aligned} \hat{\epsilon}_{out} &= \left(\frac{\cos\theta e^{i\phi}}{\sqrt{2}} \hat{\rho} + \frac{\sin\theta e^{i\phi}}{\sqrt{2}} \hat{z} \right) + \frac{ie^{i\phi}}{\sqrt{2}} \hat{\phi} \\ &= \frac{1 + \cos\theta}{2} \hat{\epsilon}_+ + \frac{\sin\theta e^{i\phi}}{\sqrt{2}} \hat{z} + \frac{\cos\theta - 1}{2} e^{2i\phi} \hat{\epsilon}_-, \end{aligned} \quad (40)$$

where $\theta = \arctan(\rho/f)$ and $\hat{\epsilon}_- = (\hat{x} - i\hat{y})/\sqrt{2}$.

REFERENCES

- [1] I.J. Cirac, P. Zoller, H.J. Kimble and H. Mabuchi, "Quantum State Transfer and Entanglement Distribution among Distant Nodes in a Quantum Network", *Phys. Rev. Lett.* **78**, 3221 (1997).
- [2] L.M. Duan, M.D. Lukin, I.J. Cirac and P. Zoller, "Long-Distance Quantum Communication with Atomic Ensembles and Linear Optics", *Nature* **414**, 413 (2001).
- [3] S.M. Savage, S.L. Braunstein and D.F. Walls, "Macroscopic quantum superpositions by means of single-atom dispersion", *Opt. Lett.* **15**, 628 (1990).
- [4] W. Rosenfeld, S. Berner, J. Volz, M. Weber and H. Weinfurter, "Remote Preparation of an Atomic Quantum Memory", *Phys. Rev. Lett.* **98**, 050504 (2007).
- [5] M. Sondermann, R. Maiwald, H. Konermann, N. Lindlein, U. Peschel and G. Leuchs, "Design of a mode converter for efficient light-atom coupling in free space", *Appl. Phys. B* **89**, 489 (2007).
- [6] S.J. van Enk and H.J. Kimble, "Strongly focused light beams interacting with single atoms in free space", *Phys. Rev. A* **63**, 023809 (2001).
- [7] D.J. Wineland, W.M. Itano, J.C. Bergquist, "Absorption Spectroscopy at the Limit: Detection of a Single Atom", *Opt. Lett.* **12**, 389 (1987).
- [8] M.K. Tey, Z. Chen, S.A. Aljunid, B. Chng, F. Huber, G. Maslennikov and C. Kurtsiefer, "Strong interaction between light and a single trapped atom without the need for a cavity", *Nature Physics*, doi: 10.1038/nphys1096 (2008).
- [9] S.J. van Enk and G. Nienhuis, "Commutation Rules and Eigenvalues of Spin and Orbital Angular Momentum of Radiation Fields", *J. Mod. Opt.* **41**, 963 (1994).
- [10] B. Richards and E. Wolf, "Electromagnetic Diffraction in Optical Systems. II. Structure of the Image Field in an Aplanatic System", *Proc. Roy. Soc. A* **253**, 358 (1959).
- [11] S.J. van Enk and G. Nienhuis, "Eigenfunction description of laser beams and orbital angular momentum of light", *Opt. Comm.* **94**, 147 (1992).
- [12] M.W. Beijersbergen, L. Allen, H.E.L.O van der Veen and J.P. Woerdman, "Astigmatic laser mode converters and transfer of orbital angular momentum", *Opt. Comm.* **96**, 123 (1993).
- [13] C. Cohen-Tannoudji, G. Grynberg and J. Dupont-Roc, *Atom-Photon Interactions: Basic Processes and Application* (Wiley, New York 1992).
- [14] S.J. van Enk, "Atoms, dipole waves, and strongly focused light beams", *Phys. Rev. A* **69**, 043813 (2004).
- [15] I. Gerhardt, G. Wrigge, P. Bushev, G. Zumofen, M. Agio, R. Pfab, and V. Sandoghdar, "Strong Extinction of a Laser Beam by a Single Molecule", *Phys. Rev. Lett.* **98**, 033601 (2007).
- [16] G. Wrigge, I. Gerhardt, J. Hwang, G. Zumofen, and V. Sandoghdar, "Efficient coupling of photons to a single molecule and the observation of its resonance fluorescence", *Nature Physics* **4**, 60 (2008).
- [17] A. Vamivakas et al. "Strong Extinction of a Far-Field Laser Beam by a Single Quantum Dot", *Nano Letters* **7**, 2892 (2007).
- [18] G. Zumofen, N.M. Mojarad, V. Sandoghdar, and M. Agio, " Perfect Reflection of Light by an Oscillating Dipole", *Phys. Rev. Lett.* **101**, 180404 (2008).